Comparative Analysis of Terahertz Propagation Under Dust Storm Conditions on Mars and Earth

Lasantha Thakshila Wedage, *Student Member, IEEE*, Bernard Butler, *Senior Member, IEEE*, Sasitharan Balasubramaniam, *Senior Member, IEEE*, Yevgeni Koucheryavy, *Senior Member, IEEE*, and Mehmet C. Vuran, *Member, IEEE*

***Abstract*—Reliable Terahertz (THz) links are necessary for outdoor point-to-point communication with the exponential growth of wireless data traffic. This study presents a modified Monte Carlo simulation procedure for estimating THz link attenuation due to multiple scattering by charged dust particles on the THz beam propagation path. Scattering models are developed for beams through dust, based on Mie and Rayleigh approximations for corresponding frequencies on Earth (0.24 THz) and Mars (0.24 & 1.64 THz). The simulation results are compared, considering parameters such as the number of Monte-Carlo photon (MCP) packets, visibility, dust particle placement density along the beam, frequency, and distance between the transmitter and the receiver. Moreover, a channel capacity model was proposed, considering THz link attenuation due to dust storms, spreading loss, and molecular absorption loss for Earth and Mars outdoor environments. Simulation results for Earth show that the link attenuation increases with dust particle placement density, distance, and frequency, and attenuation decreases with visibility and MCP packets. On Mars, similar results are obtained for both frequencies, except that the attenuation varies around a constant value with the frequency increase. Moreover, attenuation is slightly higher at 0.24 THz frequency compared to 1.64 THz when more dust particles are present on the beam propagation path. Channel capacity is estimated for Earth and Mars environments considering time and distance-dependent scenarios. Time windows that show a sudden drop of dust particles along the beam provide opportunities to communicate with high reliability. Moreover, increasing the distance between the transmitter and receiver severely reduces the channel capacity measurement in strong dust storm conditions in both environments. Our study has found that weak dust storms have relatively little effect on Mars but much more significant effects on Earth.**

***Index Terms*—Atmospheric impact on attenuation, THz Communication, scattering.**

Manuscript received 9 December 2022; revised 12 April 2023 and 31 May 2023; accepted 31 May 2023. Date of publication 13 June 2023; date of current version 13 October 2023. This work was supported in part by the Science Foundation Ireland (SFI), in part by the Department of Agriculture, Food and the Marine, Ireland on behalf of the Government of Ireland under Grant 16/RC/3835 - VistaMilk, in part by the YL Verkot, Finland, and in part by U.S. National Science Foundation under Grant ECCS-2030272. The guest editor coordinating the review of this manuscript and approving it for publication was Prof. Josep Miquel Jornet. *(Corresponding author: Lasantha Thakshila Wedage.)*

Lasantha Thakshila Wedage and Bernard Butler are with the Walton Institute, South East Technological University, X91 HE36 Waterford, Ireland (e-mail: thakshila.wedage@waltoninstitute.ie; bernard.butler@setu.ie).

Sasitharan Balasubramaniam and Mehmet C. Vuran are with the University of Nebraska-Lincoln, Lincoln, NE 68588 USA (e-mail: sasi@unl.edu; mcv@unl.edu).

Yevgeni Koucheryavy is with the Tampere University of Technology, 33100 Tampere, Finland (e-mail: yevgeni.koucheryavy@yl-verkot.com).

Digital Object Identifier 10.1109/JSTSP.2023.3285450

I. Introduction

SIXTH generation (6G) wireless networks aim to push the frequency spectrum into the Terahertz (THz) band to fulfill rising capacity demands and requirements, given the opportunity for higher bandwidths [1], [2], [3]. The 0.1 to 10 THz frequency range has the potential to (1) realize high bandwidth transmissions that can allow hundreds of GB/s data rates for communication [4], [5], [6], and (2) provide new opportunities to create miniature THz-enabled antennas due to the small wavelengths (30 μm – 3 mm), enabling us to design arrays with a large number of antenna units [7], [8], [9].

Numerous studies have shown that specific THz frequencies suffer high molecular absorption due to atmospheric gases (e.g., water vapour and oxygen). However, given the wavelength and high-energy photons of THz signals, other particles can also significantly impact the link budget, resulting in scattering and absorption of signal power.

Recent studies have shown that solid particles such as dust [10], [11], [12], [13], [14], [15], and [16], and snow [17], [18] affect THz signals, in addition to molecular absorption from atmospheric gases [19]. However, past studies have paid little attention to signal attenuation caused by solid particle movements, such as dust and sand. Therefore, further investigation is required to determine how dynamic environments composed of solid particles, such as dust storms, affect THz links. This requires further research, especially as we expand connectivity in rural areas and other planets (e.g., Mars) to an interplanetary scale. In the case of Mars, the recent vision of colonizing the planet will require high-bandwidth connectivity to maximize chances for human survival [20].

A dust storm is a meteorological phenomenon in which strong horizontal and vertical wind velocity components blow dust and sand particles from the ground into the air, creating a cloud of dust that reduces visibility and can cause damage to property, infrastructure, health and *communication*. Dust storms are more frequently found in arid regions such as the Middle East [21], North China [22], and North Africa [23] at specific periods of the year. In more densely populated areas, human activity creates dust when burning fossil fuels for heating, cooking, or transport. Considering the different environmental conditions, this study compares the effects of solid dust particles on THz and sub-THz frequencies for both Earth and Mars. Considering the differences in atmospheric conditions on Earth and Mars, with or without dust, suggests using different frequencies to enable relatively

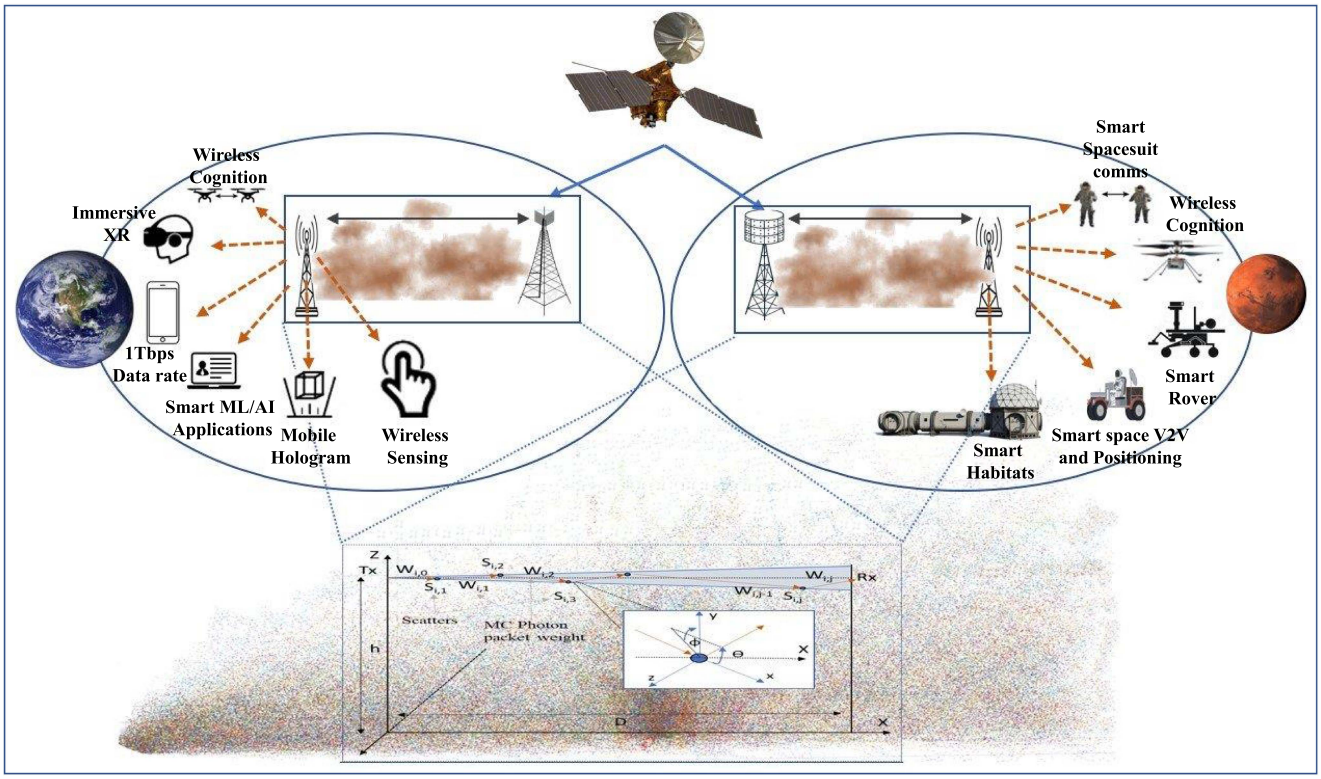

Fig. 1. THz wireless communication applications for Earth and Mars atmospheric and environmental conditions.

long-distance wireless communication on both planets. Dust storms are one of the most remarkable features on Mars. Even though wind speed on Mars is not significantly higher than on Earth, the extremely dry, dusty surface yields more dust storms. Fig. 1 provides an overview of selected wireless communications applications on Earth and proposed wireless communication applications on Mars.

In an environment where the dust particle density is higher than usual, the effects of multiple scattering of EM waves due to dust particles are non-negligible. Recent studies have not considered this significant effect of multiple scattering on the attenuation of EM waves [11], [24]. The lack of consideration of multiple scattering effects can result in significant gaps between theoretical and experimental results. This paper considers multiple scattering of EM waves due to charged dust particles along the beam propagation path. To this end, we model the EM wave as a ***photon packet*** instead of a shower of photons [25]. A photon packet models a portion of the *energy weight* of the EM wave rather than single photons, which have quantum behaviour. Therefore, we can consider an EM wave as a collection of energy packets and model multiple scattering effects utilizing the Monte Carlo algorithm to infer the radiative transfer equation. Our aim is to model the scattering behaviour of THz photons down to the single dust particle level, in order to determine their impact on the overall attenuation. The THz link scattering loss measurement in this study is inspired by [10], where the scattering loss due to charged dust particles is calculated by considering the energy of the transmitting signal as Monte Carlo Photon Packets. While, vertical THz attenuation is investigated in [10], this study considers horizontal point-to-point communication for both Earth and Mars in dusty atmospheric scenarios.

The contributions of this paper are:

1) A 3-D geometric scattering model for multiple photon-dust particle interactions is presented, using both Mie and Rayleigh approximations, to estimate the probability that a photon packet arrives at the receiver.
2) The model is used in simulations to estimate the overall channel capacity considering THz and sub-THz link budget degradation due to the combination of scattering by charged dust particles, molecular absorption loss due to the atmosphere, and free-space spreading loss.
3) Different communication channel conditions on Earth and Mars and their effect on channel capacity, including power loss caused by multiple scattering by dust, are compared and analysed.

The rest of this paper is organized as follows: Section II describes dust conditions and how they affect EM propagation and contrasts the conditions that prevail on Earth and Mars; Section III describes how 3D dust storm simulation is affected by the number of dust particles on the EM wave propagation path. Then Section IV explains the Monte-Carlo simulation process for calculating the transmittance/attenuation when photon packets are scattered by multiple dust particles. Section V presents estimates of transmittance/attenuation obtained by Monte-Carlo simulation in various parameter settings. Section VI presents a channel capacity model that combines the effect of spreading,

molecular absorption, and multiple scattering by dust, with simulated results. Finally, Section VII presents our conclusions.

II. Background

A. THz Link Behaviour in Dust Storms

THz signal attenuation due to the scattering loss caused by high dust particle density on the THz beam propagation path is the main concern of this study. Dust particle density on Mars is expected to be higher than on Earth because of the dusty atmosphere with low water vapour concentration. Mars dust consists of basalt and montmorillonite clay [26]. On the other hand, Earth dust consists of pollen, bacteria, smoke, ash, salt crystals from the ocean, and small amounts of dirt or various rocks, including sand. Moreover, during dust storm conditions on Mars, the effective radius of the dust particle varies from 1 to 4 microns with an effective variance of 0.2 – 0.4 [27]. However, the effective radius on Earth varies between 1 and 150 microns [10], [26].

Many researchers investigated the THz [10], [11], [12], [13] and lower frequency bands [14], [15] attenuation due to the presence of dust particles on the beam propagation path. In [10], Monte-Carlo simulation was used to calculate the transmittance of EM waves when they propagate through dust, considering multiple scattering effects for charged particles in 20 and 75 GHz frequencies. Hongxia et al. [12] also studied the attenuation characteristics of THz waves subject to multiple scattering caused by dust storms in the Tengger desert, using the *Mie* scattering approximation through Monte Carlo simulation. In addition, considering the Mie theory, Diao et al. [11] investigated THz wave attenuation due to heavy dust in the Martian atmosphere in the 0.1-1 THz frequency range and compared it with Earth measurements. In [13], attenuation at 0.625 THz caused by dust utilising an experimental setup found that degradation of the THz link budget is minor due to dust, compared to that found using IR beams with 1.5 μm wavelength, and average attenuation of the THz link is proportional to the dust particle density. Moreover, Elshaikh et al. [14] developed a mathematical model to characterise the microwave attenuation due to dust, considering parameters such as visibility, frequency, particle size, and complex permittivity. Li et al. [15] investigated the visible light scattering properties of partially charged dust particles utilising Mie scattering theory and found that for higher frequency (400–700 THz) EM waves in the visible spectrum, the attenuation effect of charge carried by sand particles can be ignored. Furthermore, [16] presents the EM scattering properties of the small partially charged sand/dust particles, using the Rayleigh approximation, for microwave frequencies. Additionally, in [28], [29], [30], stochastic models have been used to infer the wireless channel models propagating through particles considering multiple scattering and absorption. However, there are limited studies on wireless THz link attenuation behaviour due to *multiple* scattering of charged dust particles in combination with atmospheric conditions for Earth and Mars. At the same time, given the relative size comparison between the THz wavelength and dust particle size, it is also important to consider different approximations, such as Mie and Rayleigh, to determine the attenuation effect at a single particle level.

TABLE I
Atmospheric Gas Composition Comparison Between Earth and Mars [11] (Ppm is a Concentration of Parts Per Million)

Gas	Composition on Earth	Composition on Mars
N_2	78.084%	2.7%
O_2	20.946%	0.13%
Ar	0.93%	1.6%
H_2O	1-3%	100-400ppm
CO_2	0.003%	95.32%
CH_4	1.5ppm	-
SO_2	1ppm	-
O_3	0.05ppm	0.1ppm
N_2O	0.02ppm	-
CO	0.01ppm	0.08%
NH_3	0.01ppm	-
NO	-	100ppm

B. Atmospheric Condition Differences Between Mars and Earth

When THz EM waved pass through the atmosphere, they experience attenuation due to many factors, which differ in their impact between Earth and Mars. This study focuses on point-to-point signal degradation in the lower part of the troposphere on Earth and Mars when communicating antennas are placed 50 meters above the ground. Apart from improved line-of-sight properties, [20] shows that longer communication distances can be achieved on Mars because dust particle density decreases with height. The propagation medium in the troposphere of both planets includes gases, water vapour, clouds, fog, ice, dust, and assorted aerosols (haze), but the proportions vary. The impairment mechanisms include absorption, scattering, refraction, diffraction, multi-path, scintillation, and Doppler shift. Impairment phenomena include fading, attenuation, depolarization, frequency broadening, and ray bending. However, this study considers only Line-of-Sight (LoS) transmission under dust storm scenarios through Earth's and Mars's troposphere. It considers signal attenuation based on three factors: 1) free space path loss (which is the same for Earth and Mars), 2) molecular absorption due to atmospheric gases (which are different for Earth and Mars), and 3) scattering loss due to dust particles along the propagation path (Mars and Earth typically have different dust distributions). Free space path loss occurs due to misalignment between the transmitter and the receiver antennas. It is the same for both environments because it only depends on the carrier frequency and distance. Molecular absorption loss plays a significant role on both planets. It measures the fraction of power loss of the carrier wave that is converted to kinetic energy due to molecular vibration when EM waves propagate through molecules of the atmosphere. Therefore, unlike spreading loss, molecular absorption loss depends on local atmospheric gas composition and density (see Table I), including the carrier frequency used and distances between the transmitter and the receiver. According to [31], certain frequencies of the THz spectrum, such as 183, 325, 380, 450, 550, and 760 GHz, suffer attenuation that is significantly greater than the free space propagation loss, due to water vapour absorption on Earth. However,

the Martian atmosphere contains only about 1/1,000 as much water as Earth's. Still, even this tiny amount can condense out, forming clouds that ride high in the atmosphere or swirl around the slopes of towering volcanoes [26]. This serious issue needs to be considered for vertical communication of Mars surface devices (Rovers, Habitats, etc.) and satellites. Since our study focuses on horizontal point-to-point communication, we do not need to consider the upper atmospheric layer's impact on THz signal transmission. Therefore, at these frequencies, we expect lower molecular absorption loss and higher channel capacity on Mars than Earth.

C. Vertical vs Horizontal Communications on Mars and Earth

Although we are interested in horizontal communication on Mars, our understanding of it is limited due to the lack of research. Therefore, we focus on discussing vertical transmission instead. According to NASA, Mars rovers currently use the X band (8–12 GHz) to communicate with orbiters and Earth for Deep Space Networks. They emphasised that 44 dB attenuation can be expected due to dust when establishing vertical Surface-to-Orbiter communication utilising X-band at 10 GHz through a dust storm over a one-way 20 km path [32]. The attenuation is typically 13 dB when communicating through the same distance path of 20 km using the 2 - 4 GHz S-band. Furthermore, in [32], Ho et al. claimed that when a spacecraft lands in the southern hemisphere, at least a 3-dB margin should be considered for the Lander and Rover communication due to Martian dust storms, which result in 3 dB attenuation on the 27 – 40 GHz Ka-band radio wave for 11 km distance. However, Smith et al. found that in the worst-case scenario of severe dust storms, in which large dust particles of 20 microns in size are lifted into the atmosphere, can result in attenuation as small as 1.3 dB on Mars when utilising the Ka-band 32 GHz frequency for vertical communication with a distance of 10 km [33]. The main reason for this comparatively lower attenuation due to dust on Mars for vertical communications is that the Martian atmosphere becomes thinner as altitude increases, so molecular absorption and dust particle density decrease, resulting in higher visibility. Thus, effective *vertical* communication distances would be larger than those encountered *horizontally*. Therefore, when considering the communication distances and attenuation, utilising frequency ranges below the V-band for vertical communication on Mars is more suitable than higher frequencies.

Although the works discussed so far have focused on vertical communication, Islam et al. investigated the signal attenuation from S-Band to W-band frequencies for horizontal point-to-point communication on Earth [34]. Based on Table II, we can see that the attenuation increases dramatically with frequency. This behaviour is also similar to what we found in our study for the THz frequencies that we have considered. In particular, the attenuation is extremely high compared to those experienced at lower frequencies, due to the wavelength of the selected frequencies being approximately equal to the dust particle sizes, which creates more substantial scattering loss, resulting in higher attenuation.Even though a number of studies have investigated the THz wave propagation on Earth and Martian environments [11], [20], to the best of our knowledge, this is the first study that investigates attenuation at THz frequencies due to dust movements and applying Monte Carlo simulation using Mie and Rayleigh approximations. This will allow us to understand the behaviour of photon packets interactions at the single dust particle level, so we can understand the signal dynamics through different dust density movements. We then build on this to develop a channel capacity model that includes the effect of spreading loss, and molecular absorption loss due to atmospheric gases on each planet (see Table I) in combination with the multiple scattering losses due to dust particles.

TABLE II
COMPARISON OF VERTICAL AND HORIZONTAL COMMUNICATION ON EARTH AND MARS ENVIRONMENTS USING FREQUENCIES BELOW THZ BANDS, WHERE A= AVERAGE, W = WOST-CASE, AND τ IS THE OPTICAL DEPTH

Planet	Comms	Frequency	Visibility	Dust radius (μm)	Attenuation due to dust (dB/km)	References
Mars	Vertical	S-band	184 m	2 (a) - 20 (w)	0.65	[32]
		X-band (10 GHz)	184 m	3 (a) - 20 (w)	2.2	[32]
		Ka-band (32 GHz)	184 m	1 - 10 (w)	0.27	[32]
		Ka-band (32 GHz)	τ=6	4 (a) - 10 (w)	0.13	[33]
Earth	Horizontal	S-band	100 m	50	0.01 - 0.05	[34]
		X-band	100 m	50	0.01 - 0.1	[34]
		Ku-band	100 m	50	0.01-0.5	[34]
		K-band	100 m	50	0.01-1	[34]
		Ka-band	100 m	50	0.01-2	[34]
		W-band	100 m	50	0.01 - 5	[34]

III. THz Beam Propagation Through a Simulated 3D Dust Storm

This section discusses THz wave propagation through a randomly simulated 3D dust storm caused by wind from both vertical up-draught and horizontal velocity components. When the THz $pencil - thin$ beam propagates through a dust storm environment, a certain number of dust particles are carried in the beam propagation path (conical dust zone) by the horizontal and vertical wind components. Thus, following the dust particles' trajectory, we calculated the number of dust particles present in the conical dust zone. The simulated dust storm (see Fig. 2) consists of a line source starting at $X = 0$ and a vertical upward movement of dust based on the vertex motion due to wind turbulence. The line source dust storm in this study spreads for 8 m along the Y-axis $(-4 \leq Y \leq 4)$. Such a line source is more realistic than a point source for dust storm simulation on both Earth and Mars.

MATLAB's wind package was used to simulate the storm and considered an exponential movement of dust along the positive X-axis coupled with the strong wind in the same direction. Also, dust particles gradually precipitate from the atmosphere when their weight exceeds upward forces. The movement of dust particles from a point source dust storm downstream involves both an upward wind and a horizontal wind, mixing to create a vortex flow that resembles a whirlwind.

When counting the dust particles on the conical dust zone, we utilised the following methods. We aim to determine how the dust particles are moving within a cloud, so we modelled and simulated the movement of dust particles in a 1 km long *thin* conical dust zone. The reason for considering a thin dust zone

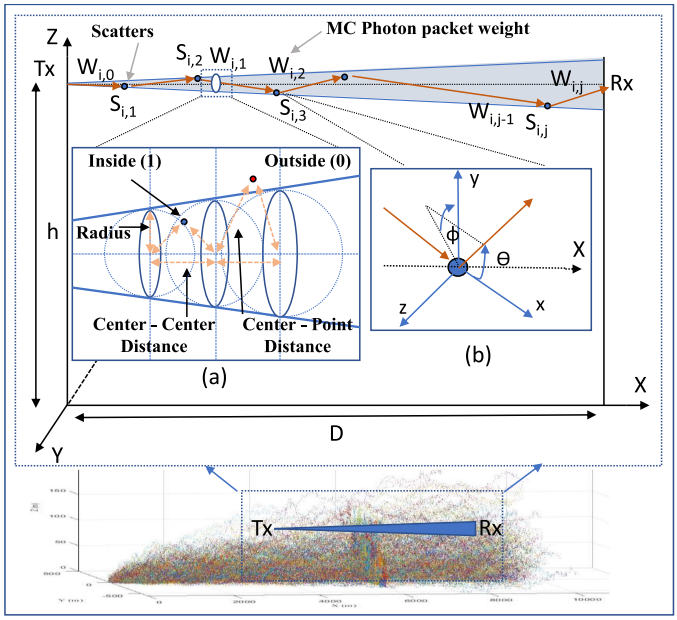

Fig. 2. Multiple scattering processes of electromagnetic waves through a sand/dust storm considering (a) the trajectory and mobility of dust particles through the conical dust zone, and (b) a single dust particle coordinate system to infer scattering behaviour.

is to suggest this model for the entire THz spectrum of 0.1 to 10 THz. We considered a scenario with a 1 km-long dust zone with the starting point (5500,0,50) and ending point (6500,0,50) and a point source dust devil at the midway point (6000,0,0). We excluded from the simulation those dust particles whose height was less than h-1 (h is the transmitter antenna height in m) to reduce computation time. All particles whose height was greater than h-1 were included to simulate realistic cases where particles fall back into the geometric volume of the dust zone over time. Then we counted dust particles inside the conical dust zone by subdividing the cone into cylindrical disks having a very short distance of 1 cm between the neighbouring centres (see Fig. 2(a)) and encoded each dust particle (1: inside, 0: outside), by computing the instantaneous position of the particle relative to the nearest cylindrical region. As a result, we found that there are approximately 100 dust particles per 10 m of a 1 km long conical dust zone. Also, we found that the ratio of the number of dust particles within the 1 km long dust zone, relative to the number of dust particles in the generated local dust storm for that environment, is 0.0022872.

Thus, we determined this for Earth and considered 100 times more dust particles for Mars, considering the blockage area (See Section VI). We utilised these measurements in our study due to the lack of literature that discusses the dust density measurements on Earth and Mars. We then utilised these measurements to infer the behaviour of the THz links by varying the distance between the transmitter and the receiver from 1 m to a maximum of 200 m for both Earth and Mars environments, by also considering a number of different scenarios.

IV. Modelling Monte Carlo Photon Packets Propagation Through Dust Particles

In this section, we calculate the transmittance and the corresponding attenuation of the THz EM wave when it propagates through suspended charged dust particles. The initial intention was to consider the THz EM wave as a collection of photons. However, photon position and trajectory are not Physically meaningful here [25], but collections of photons enable us to discretize the beam in a physically meaningful way. Monte Carlo simulation is used to estimate transmittance, where the incident plane EM wave is discretized as Monte Carlo photon (MCP) packets/units. Such photon packets provide an appropriate physical unit for discrete event simulation [10]. Each MCP packet is considered to be an equally divided portion of the energy weight of the EM wave field. In this simulation model, we assume that the particle number concentration is uniformly distributed throughout the THz beam area, and dust particles are randomly positioned.

The intensity (I) of the incident THz EM wave can be expressed as $I_0 = M.W$, where M is the number of MCP packets per unit area per unit time and W is the energy weight of each MCP. Here, we assume that MCP packet i $(i = 1, 2, \ldots, M)$ is randomly scattered by dust particles j before it either exits the geometric volume of the dust zone (beam) or reaches the receiver interface boundary at $X = D$. We assume that MCP packets enter from the point $(0, 0, h)$ (where h is the transmitter antenna height) (see Fig. 2) and are forward-scattered by scattering particles $S_{i,l}$ $(l = 1, 2, \ldots, j)$ whose positions are denoted by $(x_{i,l}, y_{i,l}, z_{i,l})$, which are assumed random. Moreover, the algorithm will randomly select the number of scattering particles (l) that collide with an MCP packet from j dust particles on the EM wave propagation path. This approach is employed to account for the impracticality of MCP packets colliding with every dust particle. Therefore, we assume that each scattering event occurs at the particle's position and deflects the MCP packet's propagation direction. This process continues until the last scattering event, while the remaining dust particles are assumed to be uniformly distributed along the beam path.

We suppose the initial energy weight of each MCP packet is $W = W_{i,0} = 1$ and after scattering due to scattering particle $S_{i,l}$ it becomes $W_{i,l}$. We also define a local coordinate system xyz with the origin located at the scattering particle. So, we can define the propagation direction of the MCP packet i with respect to the local coordinate system xyz, which is to the x direction considering forward scattering. The propagation direction for the scattering direction of the MCP packet i due to the impact with scattering particle $S_{i,l}$ can be expressed using the direction cosines $(\mu^x_{i,l}, \mu^y_{i,l}, \mu^z_{i,l})$ in the global coordinate system XYZ, which is defined with the help of scattering (or deflection) angle θ and azimuth angle ϕ (see Fig. 2(b)). The direction cosines were determined in every simulated collision by evaluating the scattering particle position $(x_{i,l}, y_{i,l}, z_{i,l})$, and the propagation angles (θ, ϕ). This evaluation was performed using randomly generated uniformly distributed numbers for the global coordinate system, and further explanation will be provided later. Direction cosines can be calculated according to

Fig. 2(b) as follows,

$$\mu^x_{i,l} = -sin(\theta_{i,l})cos(\phi_{i,l})\sqrt{1-(\mu^x_{i,l-1})^2} + \mu^x_{i,l-1}cos(\theta_{i,l}) \tag{1a}$$

$$\mu^y_{i,l} = \frac{sin(\theta_{i,l})(\mu^y_{i,l-1}\mu^x_{i,l-1}cos(\phi_{i,l}) - \mu^z_{i,l-1}sin(\phi_{i,l}))}{\sqrt{1-(\mu^x_{i,l-1})^2}} + \mu^y_{i,l-1}cos(\theta_{i,l}) \tag{1b}$$

$$\mu^z_{i,l} = \frac{sin(\theta_{i,l})(\mu^z_{i,l-1}\mu^x_{i,l-1}cos(\phi_{i,l}) + \mu^y_{i,l-1}sin(\phi_{i,l}))}{\sqrt{1-(\mu^x_{i,l-1})^2}} + \mu^z_{i,l-1}cos(\theta_{i,l}). \tag{1c}$$

If $|\mu^x_{i,l-1}| > 0.99999$, then

$$\mu^x_{i,l} = \frac{\mu^x_{i,l-1}}{|\mu^x_{i,l-1}|}cos(\theta_{i,l}) \tag{2a}$$

$$\mu^y_{i,l} = sin(\theta_{i,l})cos(\phi_{i,l}) \tag{2b}$$

$$\mu^z_{i,l} = sin(\theta_{i,l})sin(\phi_{i,l}) \tag{2c}$$

In the initial stage, we suppose that the MCP packet i enters the dust particle zone from $X = 0$ at point (0,0,h) and propagates along the direction of $(\mu^x_{i,0}, \mu^y_{i,0}, \mu^z_{i,0}) = (1, 0, 0)$. The simulation process depends on uniformly-distributed, randomly generated numbers $\epsilon_{i,l}, \nu_{i,l}$, and $\chi_{i,l} \sim Uniform(0, 1)$, which are used to calculate the random variables $\Delta S_{i,l}, \theta_{i,l}$ and $\phi_{i,l}$.

The $\Delta S_{i,l}$ is the travelling distance between the scattering particles $S_{i,l}$ and $S_{i,l-1}$ and in [10] this is defined as,

$$\Delta S_{i,l} = \frac{-ln(\epsilon_{i,l})}{C_{ext}} \tag{3}$$

where C_{ext} is the total extinction cross-section efficiency of spherical dust particles with radius r. The total extinction cross-section efficiency is expressed [10] as,

$$C_{ext} = \int_{r_{min}}^{r_{max}} N_0 P(r) c_{ext} d(r), \tag{4}$$

where $P(r)$ is the log-normal size distribution of dust particles for both Earth [35] and Mars [11] environments. Here, N_0 is the number of dust particles per unit volume, and it can be expressed as a function of visibility (V_b) [11], which is represented as,

$$N_0 = \frac{15}{0.034744 V_b \int_0^{2r_{max}} \pi r^2 P(r) dr}. \tag{5}$$

On Earth, dust particle radius varies between 1 to 150 μm. Therefore, when considering the approximate equality of the effective diameter of the dust particles and the wavelength of the THz frequency utilised in this study, we can use the Mie approximation [36] to infer the total extinction cross-section (c_{ext}) [26], which is the sum of the absorption cross-section and scattering cross-section. The c_{ext} is expressed by the Mie solution for spherical particles with dielectric constant ϵ [14] as,

$$c_{ext} = \frac{k^3 r \lambda^2}{2}(c_1 + c_2(kr)^2 + c_3(kr)^3) \tag{6}$$

where,

$$c_1 = \frac{6\epsilon''}{(\epsilon'+2)^2 + (\epsilon'')^2} \tag{7a}$$

$$c_2 = \epsilon'' \left\{ \frac{6}{5} \frac{7(\epsilon')^2 + 7(\epsilon'')^2 + 4\epsilon' - 20}{[(\epsilon'+2)^2 + (\epsilon'')^2]^2} \right\} + \frac{1}{15} + \frac{5}{3[(2\epsilon'+3)^2 + 4(\epsilon'')^2]^2} \tag{7b}$$

$$c_3 = \frac{4}{3} \left\{ \frac{(\epsilon'-1)^2(\epsilon'+2) + [2(\epsilon'-1)(\epsilon'+2) - 9] + (\epsilon'')^4}{[(\epsilon'+2)^2 + (\epsilon'')^2]^2} \right\}. \tag{7c}$$

The complex refractive index of dry dust particles on Earth can be expressed as $\sqrt{3 + \imath.\frac{18.256}{f}}$ [12], where f is the frequency and $\imath$ is the imaginary unit $\sqrt{-1}$.

On the other hand, the total extinction cross-section of the dust particles on Mars can be evaluated utilising the Rayleigh approximations [16] because the effective diameter of the dust particles on Mars (1-8 μm) is less than one-tenth of the wavelength of the frequency [37] used in this study. Therefore, the total extinction cross-section can be expressed as,

$$c_{ext} = \frac{8}{3}\pi k^4 r^6 \left|\frac{\epsilon_r - 1}{\epsilon_r + 2}\right|^2 + 12\pi k \epsilon''_r r^3 \frac{1}{|\epsilon_r + 2|^2} + \frac{\pi}{6}\frac{k^4 r^6 \sigma^2}{E_0^2 \epsilon_0^2}|\epsilon_r - 1|^2 \sin^2(\theta_q) \tag{8}$$

where ϵ_r and ϵ_0 are the relative permittivities of the particle and the vacuum, $k = \frac{2\pi}{\lambda}$ is the wave number, and $2\theta_q$ explains the angle of the spherical cap of the electric charges distribution [16]. Since all the dust particles become charged in a dust storm, we take $\theta_q = \frac{\pi}{2}$ assuming that the electric charges are distributed over the whole surface of the particle [38]. The Surface charge density can be expressed as $\sigma = \frac{2Q_m r\rho}{3(1-\cos(\theta_q))}$, where Q_m is the charge-mass ratio (-300 μC/kg [16]), and ρ is the particle mass density of dust on Mars (2370 kg/m^3 [39]). Since the surface charge density varies with the dust particle radius (0.5–4 microns), we have taken it to randomly vary between $(-1.896, -0.237)$ μC/m^2 for Mars. Moreover, we can take the complex refractive index of dust particles on Mars as $1.52 + 0.01i$ [11], [20] corresponding to the radius range (0.5–4 μm) used in this study.

The scattering angle, $\theta_{i,l}$, due to the i^{th} MCP packet impact with scatter l is represented as,

$$\theta_{i,l} = \begin{cases} cos^{-1}\left\{\frac{1}{2g}\left((1+g^2) - \left(\frac{1-g^2}{1-g+2g\nu_{i,l}}\right)^2\right)\right\} \\ \quad \text{for } g \neq 0 \\ cos^{-1}(2\nu_{i,l} - 1) \text{ for } g = 0 \end{cases} \tag{9}$$

where $\phi_{i,l}$ is the azimuth angle due to the same impact and

$$\phi_{i,l} = 2\pi\chi_{i,l} \tag{10}$$

and $g =< cos(\theta) > \in [0, 1]$ is the asymmetry factor (here, $g = 0$ refers to the isotropic scattering and 1 refers to forward direct

scattering). We assume g varies uniformly between 0.5 and 1 for our simulations which is the average value for the direct forward scattering.

After calculating the random variables $\epsilon_{i,l}, \nu_{i,l}$, and $\chi_{i,l}$, we can determine the (random) position of the scattering particle $S_{i,j}$ $(X_{i,l}, Y_{i,l}, Z_{i,l})$ in the global coordinate system utilising the (1), (2), and (3) as below. The position of the scattering particles can be expressed as,

$$\begin{aligned} X_{i,l} &= X_{i,l-1} + \Delta S_{i,l}\, \mu^x_{i,l-1} \\ Y_{i,l} &= Y_{i,l-1} + \Delta S_{i,l}\, \mu^y_{i,l-1} \\ Z_{i,l} &= Z_{i,l-1} + \Delta S_{i,l}\, \mu^z_{i,l-1} \end{aligned} \tag{11}$$

Successful transmittance occurs only for MCP packets that reached the receiver interface at a distance of D from the transmitter. If $X_{i,l} >= D$, this means that $S_{i,l-1}$ is the last scattering particle encountered by the MCP packet i before it leaves the region boundary $(X = D)$ from the receiving interface. Therefore, we can stop the simulation process and go to the next MCP packet $(i + 1)$ after calculating its current energy weight $(W_{i,l})$. The energy weight follows the Beer-Lambert law, which determines how $W_{i,l-1}$ is related to the $W_{i,l}$ [10], [40]. Thus, the energy weight of an MCP packet after collision with a scattering particle can be expressed as,

$$W_{i,l} = W_{i,l-1}\, exp\left\{\frac{-C_{ext}(X_{i,l} - X_{i,l-1})}{\mu^x_{i,l-1}}\right\}. \tag{12}$$

If $X_{i,l} < D$, this means MCP packet i is unable to reach the receiver interface after impacting with l scatters. From this point, we focus our interest more on the energy weight of the MCP packet i and calculate the energy weight of the MCP packet $W_{i,l}$ using (12). In this instance, we assume that the initial energy weight of the MCP packet is a unit (i.e., $W_{i,0} = 1$), where we define a threshold (ϵ_t) value of 1×10^{-5} to consider as the minimum energy weight that an MCP packet can take after l impacts with the scatters. If the energy weight of an MCP packet does not exceed this minimum threshold (i.e., $W_{i,l} < \epsilon_t$), the packet is assumed not to reach the receiver and is recorded as such. Therefore, we can set $j = l$ and $W_{i,l} = 0$.

Based on the calculation of energy weights of the MCP packets that reached the receiver interface, we can calculate the transmittance of the THz EM wave by,

$$T_{MS} = \frac{\sum_{i=1}^{M} W_{i,l}\, exp\left\{\dfrac{-C_{ext}(D - X_{i,l})}{\mu^x_{i,l}}\right\}}{I_0}. \tag{13}$$

From our calculations, we noticed that (13) does not converge to a finite value for every simulation. Therefore, we assume the transmittance to be zero when it is divergent and set the simulation to the next Monte-Carlo process. Based on the transmittance calculations at the end of this procedure, we can calculate the specific attenuation A_{MS} in (dB/m) according to [10], as,

$$A_{MS} = \frac{-4.343\, ln(T_{MS})}{D}. \tag{14}$$

V. THz Channel Capacity

To evaluate the channel capacity in the THz band, we can decompose the received signal as a sum of the sub-bands, where each sub-band channel is narrow and has a flat-band response [41].

The i^{th} frequency sub-band is defined as $\Delta f_i = f_{i+1} - f_i$ with power P_i under the constraint $\sum_{i=1}^{N_B} P_i \leq P_t$, where N_B refers to the total number of sub-bands, and P_t stands for the total transmit power. In the i^{th} narrow-band, the sub-band capacity, C_i, is expressed in [41] as,

$$C_i = \Delta f_i \log\left(1 + \frac{|h_{LoS}|^2 P_i}{\Delta f_i S_D(f_i)}\right), \tag{15}$$

where S_D is the power spectral density of the additive white Gaussian noise (AWGN) and h_{LoS} is the frequency-dependent channel response for attenuation due to dust particles, including spreading loss and molecular absorption loss due to gas molecules on the LoS signal propagation path. According to [41], h_{LoS} can be expressed as,

$$h_{LoS}(\tau) = \alpha_{Los}\delta(\tau - \tau_{LoS}). \tag{16}$$

where α_{Los} refers to the attenuation and τ_{LoS} refers to the propagation delay due to dust particles and gas molecules on the signal propagation path, and $\tau_{LoS} = \dfrac{d_{LoS}}{c}$. Where d_{LoS} is the signal travelling distance through dust, which is D in this study, because we calculate the transmittance using the MCP packets that reached the fixed receiver interface. Also, the power spectral density of AWGN can be expressed as $S_D(\tau) = \frac{n_0}{2}\delta(\tau)$ and, in the frequency domain, $PSD(S_D(f))= \frac{n_0}{2}$. Utilizing the Wiener-Khinchin theorem, the frequency-dependent channel response for LoS attenuation can be expressed as [41],

$$h_{LoS}(\tau) = |H_{LoS}(f)|\delta(\tau - \tau_{LoS}). \tag{17}$$

The free space direct ray or LoS channel transfer function, H_{LoS}, consists of the spreading loss function (H_{Spr}), the molecular absorption loss function (H_{Abs}), and scattering loss function due to dust particles (H_{Dust}), which can be expressed as,

$$H_{LoS}(f) = H_{Spr}.H_{Abs}.H_{Dust}e^{-j2\pi f \tau_{LoS}}. \tag{18}$$

The free space path loss or the spreading loss (PL_{Spr}) measures the fraction of power lost by a beam with frequency f over a distance D in a vacuum, and it can be expressed according to [42] as,

$$PL_{spr} = \left(\frac{4\pi D f}{c}\right)^2, \tag{19}$$

where c is the speed of light in the medium. Thus, according to [41], the corresponding channel transfer function for the spreading loss can be expressed as,

$$H_{spr} = (PL_{spr})^{-1/2} = \left(\frac{c}{4\pi D f}\right). \tag{20}$$

The molecular absorption loss measures the fraction of power converted to kinetic energy due to molecular vibration when EM waves propagate through molecules in the atmosphere. Thus, when transmitting frequency f through a homogeneous medium

between a transmitter and receiver at a distance D, the molecular absorption loss is obtained with the help of the Beer-Lambert law [42], which is represented as,

$$PL_{abs} = e^{k(f)D}, \tag{21}$$

where $k(f) = \sum_{i,g} k_g^i(f)$ and $k_g^i(f)$ is the monochromatic absorption coefficient of the i^{th} isotopologue of g^{th} gas at frequency f. When calculating the absorption coefficient, we consider water vapour and nine other gases for Earth and six gases for Mars (see Table I), except for Argon. This allows us to consider the vastly different gas concentrations between the two planets. The monochromatic absorption coefficient for each isotopologue of a particular gas in the Martian and Earth atmosphere at frequency f is provided in [43],

$$k_g^i(f) = S_g^i(T) F^i(f), \tag{22}$$

where $S_g^i(T)$ is the line intensity at temperature T (210 K for Mars) referenced to the temperature 296 K of the i^{th} isotopologue of g^{th} gas, which can be easily calculated using the high-resolution transmission (HITRAN) molecular spectroscopic data. Where, F^i is the spectral line shape function at frequency f. In the lower atmosphere on Earth, pressure broadening of spectral lines dominates the line shape and a Lorentz profile can be assumed as the line shape function, and it is given by [43],

$$F_L^i(f) = \frac{1}{\pi} \frac{\gamma(p,T)}{\gamma(p,T)^2 + [f - (f_g^i + \delta(P_{ref})P)]^2} \tag{23}$$

where f_g^i is the resonant frequency for the isotopologue i of gas g, $\gamma(P,T)$ is the Lorentzian (pressure-broadened) HWHM for a gas at pressure P (atm), temperature T (K), and $\delta(P_{ref})$ is the pressure shift at reference pressure (P_{ref}= 1 atm).

Since Doppler-broadening dominates the line shape in low-pressure environments such as Martian environment, a Gaussian profile can be assumed as the line shape function, and it is given by,

$$F_G^i(f) = \sqrt{\frac{\ln 2}{\pi {\alpha_D^i}^2}} \exp\left(- \frac{(f - f_g^i)^2 \ln 2}{{\alpha_D^i}^2} \right), \tag{24}$$

where α_D^i is the Doppler broadening half-width,

$$\alpha_D^i = \frac{f_g^i}{c} \sqrt{\frac{2 N_A k_B T \ln 2}{M^i}}, \tag{25}$$

where M^i is the molar mass of isotopologues which can be obtained from the HITRAN database [43], and N_A and k_B are the Avogadro and Boltzmann constants.

Thus, according to [41], the corresponding channel transfer function for the molecular absorption loss due to the gas molecules in the atmosphere can be expressed as,

$$H_{abs} = (PL_{Abs})^{-1/2} = e^{-\frac{1}{2}k(f)D}, \tag{26}$$

Finally, H_{Dust} is the transfer function for the attenuation due to dust particles that can be expressed as following the relationship between the transfer functions and the attenuation functions for spreading loss and molecular absorption loss, respectively, as well as utilising the dust attenuation function in (14) in dB, which is represented as,

$$H_{dust} = \frac{1}{\sqrt{10^{-0.4343 \ln(T_{MS})}}}. \tag{27}$$

Therefore, substituting the functions derived for H_{Spr}, H_{Abs}, and H_{Dust}, to (18), we can calculate the channel transfer function. Moreover, in this study, we consider narrow frequency bands for each environment, which are 0.22–0.24 THz for Earth, 0.22–0.24 THz and 1.64–1.67 THz for Mars. Therefore, we can suppose that $P_i = P_t$ and the (15) can be rewritten as,

$$C = \Delta f \log\left(1 + \frac{|h_{LoS}|^2 P_t}{\Delta f S_D(f)}\right). \tag{28}$$

TABLE III
CHANNEL CONDITIONS AND SIMULATION SETTINGS FOR BOTH EARTH AND MARS

Parameter	Earth	Mars
Frequency	0.24 THz	0.24 & 1.64 THz
MCP packets	10^4	10^4
Dust Density	10^2 per $10m$	10^4 for 10 m
Dust radius	1–150 microns	0.5–4 microns
Dust size distribution	log-Normal	log-Normal
Antenna height	50 m	50 m
Approximation	Mie	Rayleigh
Distance	1 - 200 m	1 - 200 m
Temperature	288 K	210 K
Surface Pressure	1013 mb	6.1 mb
Surface density	1.29 Kg/m^3	0.02 Kg/m^3

VI. RESULTS AND DISCUSSION

A. Transmittance and Attenuation Measurements Through Monte-Carlo Simulations

This subsection presents the simulation results for the transmittance and attenuation of the THz link and the generated estimation models for the THz attenuation due to dust particles on the beam propagation path by varying parameters such as the MCP packets, visibility, dust particle number, the distance between transmitter and the receiver, and EM frequency. When simulating data for a targeted parameter, we have kept the other parameters constant to make interpretation easier (see Table III). Thus, we have chosen a frequency of 0.24 THz and 1.64 THz as the constant frequencies for Mars [20], and 0.24 THz frequency for Earth [44], [45], [46] corresponding to low molecular absorption and high transmission distance. However, it is crucial to consider molecular absorption on Mars, even though it has a thin atmosphere with very low water vapour concentration. Moreover, we have considered 100 dust particles on the beam propagation path for a 10 m fixed distance between the transmitter and receiver, as explained in Section III for simulations on Earth considering a 1 km long dust zone. It is unrealistic to consider the same number of dust particles for the Mars simulations because of the tiny particle sizes on Mars. However, due to the lack of comparable physical/meteorological data on Mars, we propose the following method as a start to estimate dust density on Mars corresponding to Earth, which should be verified with real Martian data when it becomes available. That is, to have a fair comparison of the effect of dust

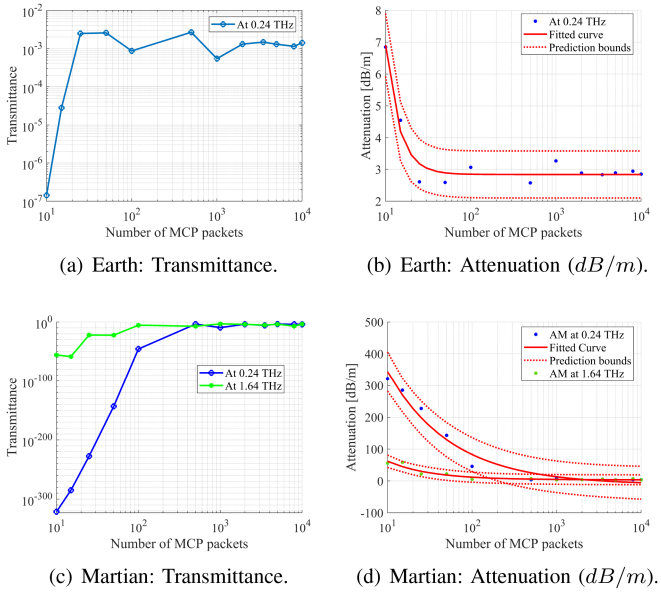

(a) Earth: Transmittance. (b) Earth: Attenuation (dB/m).

(c) Martian: Transmittance. (d) Martian: Attenuation (dB/m).

Fig. 3. Simulation measurements of the transmittance and the attenuation for a THz beam with frequencies of 0.24 THz for Earth ((a) and (b)) and 0.24 THz and 1.64 THz for Mars ((c) and (d)) by varying MCP packets from 10 to 10000 while fixing the dust particle number (100/10000) on the propagation path with a distance of 10 m between the transmitter and the receiver.

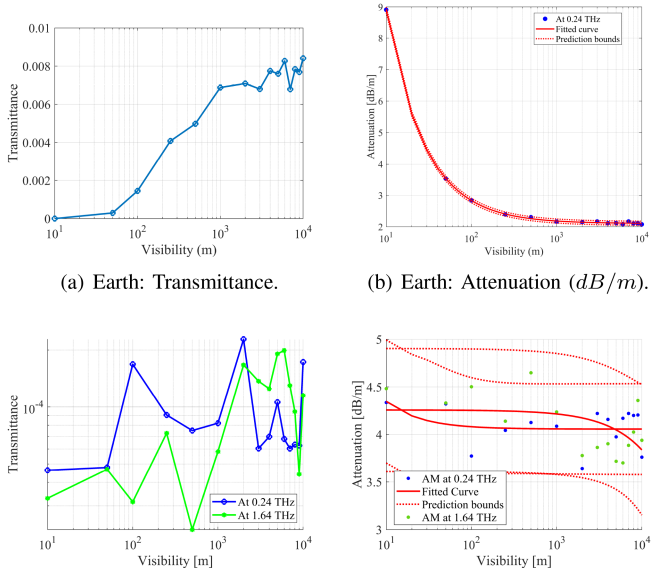

(a) Earth: Transmittance. (b) Earth: Attenuation (dB/m).

(c) Martian: Transmittance. (d) Martian: Attenuation (dB/m).

Fig. 4. Simulation measurements of the transmittance and the attenuation for a THz beam of 0.24 THz for Earth ((a) and (b)), and 0.24 THz and 1.64 THz frequency for Mars ((c) and (d)), respectively, by varying the visibility from 10 to 10000 m while fixing MCP packets (10000) and the distance (10 m) between transmitter and the receiver.

particles on the THz beam propagation path for both Earth and Mars, we assume the same blockage area for both environments.

Considering the blockage that the dust particles create and the proportional relationship between blockage area and the dust particle radius squared (i.e. Area $\propto r^2$), we consider 10,000 dust particles for Mars and 100 dust particles on Earth (i.e. 100 times more on Mars than on Earth), because the average dust particle radius on Earth is approximately 10 times greater compared to Mars so the blockage area per particle on Earth is approximately 100 times greater than that on Mars. When selecting the number of MCP packets, we considered 10000 packets in this study.

Fig. 3 illustrates the simulated data for the transmittance and the attenuation using the simulation setup explained in Section IV for Earth and Mars environments by varying the number of MCP packets from 10 to 10000, while keeping the other parameters constant. As we can see from the figures, the transmittance for both Earth and Mars environments (see Fig. 3(a) and (c)) increase rapidly when the MCP packets increase at the beginning from 10 up to 500. Moreover, we noticed higher transmittance when utilising the 1.64 THz frequency link compared to the 0.24 THz in this range due to the higher energy weight of higher frequency links. Therefore, we can expect comparably high channel capacities on Mars by utilising high THz frequency links. After that, the transmittance converges to a particular value corresponding to each environment. Furthermore, the attenuation decrease follows a power function for both Earth and Mars environments (see Fig. 3(b) and (d)) and converges approximately to a value of 3.6 dB/m and 2.8 dB/m (for 0.24 and 1.64 THz frequencies, respectively). However, the attenuation is dramatically higher at 0.24 THz frequency in the period of 10 to 500 MCP packets compared to the 1.64 THz frequency, so we can expect communication blackout on Mars when utilising 0.24 THz links for communication in a dust storm scenario. In addition, we can expect very low attenuation for a higher number of MCP packets in both environments and all considering frequencies. The fitted power function for attenuation with respect to the MCP packets (N_{MCP}) can be expressed as $\text{Attenuation}(dB/m) = 2145N_{MCP}^{-2.721} + 2.839$ for Earth at 0.24 THz frequency, $\text{Attenuation}(dB/m) = 1328N_{MCP}^{-0.5717} - 12.32$ for Mars at 0.24 THz and $\text{Attenuation}(dB/m) = 410N_{MCP}^{-0.8485} + 3.727$ for Mars at 1.64 THz.

Next, we investigated the effect of visibility on the transmittance and attenuation measurement for Earth and Mars environments by varying the parameter values from 10 to 10000 m (see Fig. 4). Generally, when the visibility increases between the transmitter and the receiver, we will see fewer dust particles on the beam propagation path with a high distance variance between the particles. Therefore, we can expect high transmittance and low attenuation when the visibility increases. According to Fig. 4(a), the transmittance of the Earth's environment are increasing dramatically, with the visibility and attenuation (see Fig. 4(b)) decreasing following a power function as expected. Moreover, the attenuation approximately converges to 2.1 dB/m value with an increase of visibility near 10000 m, which we can consider as clear sky condition. The fitted power function for the attenuation against the visibility (V) can be expressed as $\text{Attenuation}(dB/m) = 63.41\ V^{-0.9694} + 2.105$ for the Earth environment. On the other hand, the transmittance for the Mars environment (see Fig. 4(c)) shows an increasing trend for both 0.24 and 1.64 THz frequencies. However, the transmittance for certain parameter values diverges from the trend because, according to our simulation process, each MCP packet

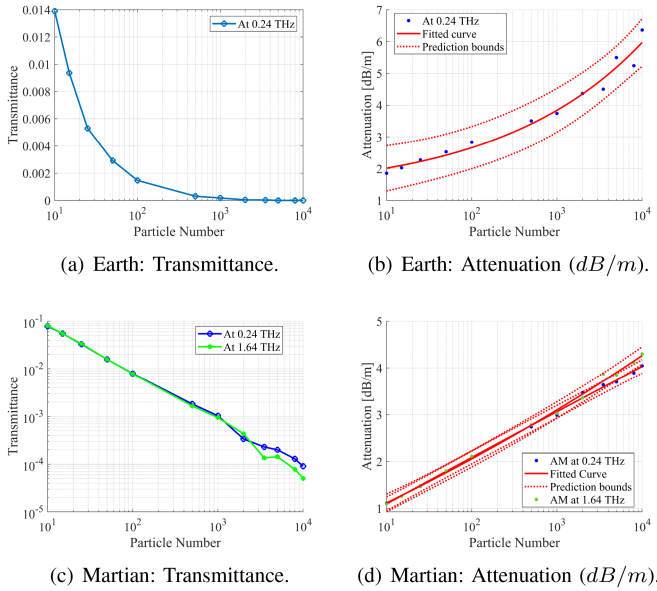

(a) Earth: Transmittance. (b) Earth: Attenuation (dB/m).

(c) Martian: Transmittance. (d) Martian: Attenuation (dB/m).

Fig. 5. Simulation measurements of the transmittance and the attenuation for a THz beam of 0.24 THz for Earth ((a) and (b)), and 0.24 THz and 1.64 THz frequency for Mars ((c) and (d)), respectively, by varying the dust particle number on the beam propagation path from 10 to 10000 with fixed number of MCP packets (10000) and the distance (10 m) between the transmitter and the receiver.

will randomly select the dust particles for collision. Therefore, we can notice a rippling behaviour of the transmittance. Even if the dust density on the beam propagation path is low, the transmittance can also be low if the collision rate with dust particles is high. Corresponding to the transmittance, we can see a slight linear decrease in attenuation on Mars at 1.64 THz frequency (see Fig. 4(d)). The fitted linear function can be expressed as $\text{Attenuation}(dB/m) = -4.184 \times 10^{-5} V + 4.256$. Meanwhile, the attenuation on Mars at 0.24 THz frequency, decreases following a power function which can be fitted as $\text{Attenuation}(dB/m) = 3.398\ V^{-1.069} + 4.056$.

The dust particle density can vary unpredictably with the wind in a dust storm on Earth and Mars. There can be time windows with very low dust particles on the beam propagation path, which will be perfect for transmission. To investigate the effect of dust particle count, we have measured the transmittance and attenuation for Earth and Mars environments by varying dust particle numbers from 10 (very low) to 10000 (very high). As shown in Fig. 5(a) and (c), the transmittance in the considered frequencies drops dramatically to near zero with the increase of dust particles for both environments. This rapid transmittance drop happens due to the high amount of scatters on the THz beam propagation path that each MCP packet should randomly collide. Thus, the attenuation (see Fig. 5(b) and (d)) increases rapidly following a power function for both environments in the considered frequencies. The fitted power function for attenuation against the dust particle number (D_{PN}) can be expressed as $\text{Attenuation}(dB/m) = 0.4423 D_{PN}^{0.2579} + 1.213$ for Earth. The attenuation and fitted curves for Mars for 0.24 THz and 1.64 THz frequencies show approximately equal behaviour up to 2000 dust particles due to the possibility of having few dust particles collide. When a large number of dust particles (>2000) are present on the beam propagation path, the attenuation is slightly higher for 1.64 THz than 0.24 THz. This is because the wavelength corresponding to the 1.64 THz link is approximately equal to the size of the dust particles on Mars than 0.24 THz, creating considerably strong energy weight losses of the MCP packets. Therefore, utilising high THz frequency links is not recommended for communication in a situation such as a global dust storm on Mars. The fitted power functions for attenuation against the dust particle number on the beam propagation path on Mars can be expressed as $\text{Attenuation}(dB/m) = -75.79 D_{PN}^{-0.005793} - 75.88$ at 0.24 THz, and $\text{Attenuation}(dB/m) = 7.534 D_{PN}^{0.04617} - 7.262$ at 1.64 THz. Furthermore, attenuation does not converge to a particular value as in previous cases when increasing the number of dust particles on the beam propagation path. Therefore, we can expect a communication blackout in a regional/global dust storm situation because it boosts the dust particle density in the communication area.

As mentioned above, dust density on the beam propagation path can vary significantly on Earth and Mars due to the unpredictable wind, temperature and pressure behaviour. Therefore, to conduct more realistic simulations, we have investigated the effect of distance between the transmitter and the receiver when we have various dust densities that vary with the distance. Dust density usually measures the number of dust particles per unit volume. However, in this study, we define it as the number of dust particles per meter for simplicity because the THz beam is assumed to be a conical shape, and its face area is tiny. For instance, if we consider 10 dust particles per meter density for 100 m, we assume that 1000 dust particles are uniformly distributed on the beam propagation path. As we can see in Fig. 6(a), the transmittance on Earth drops dramatically with distance, and when increasing the dust density, the transmittance reaches near zero rapidly beyond 100 m. However, on Mars (see Fig. 6(c)), the transmittance slightly decreases compared to Earth for both 0.24 THz and 1.64 THz frequencies. Moreover, the average transmittance in each frequency is approximately equal for the corresponding dust density. We can also clearly notice that the transmittance for higher dust densities at 0.24 THz or 1.64 THz frequency are significantly lower than the corresponding lower dust densities, as expected. However, there is little difference between the transmittance calculations for 50/m and 100/m dust densities up to 150 m for the 1.64 THz link. On the other hand, the attenuation (see Fig. 6(b) and (d)) increases with increasing distance and dust density for both environments.

Furthermore, we investigated the impact of frequency on the transmittance and attenuation on Earth and Mars. As illustrated in Fig. 7(a), the transmittance for Earth's environment decreases following an exponential function with the frequency increase from 0.1 to 4 THz. We were unable to calculate transmittance following our simulation process beyond the 4 THz frequency limit since we are considering the dust particles with a radius of 1 to 150 microns for Earth's environment, wavelengths can be comparably low or approximately equal to the dust particles' size after some frequency threshold, creating more difficulties

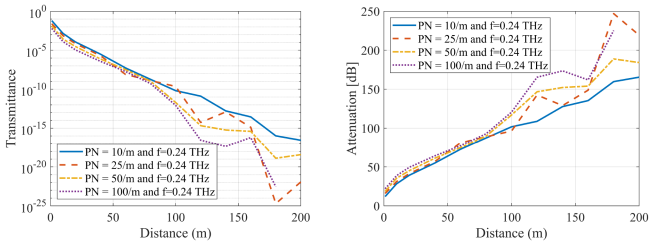

(a) Earth: Transmittance. (b) Earth: Attenuation (dB).

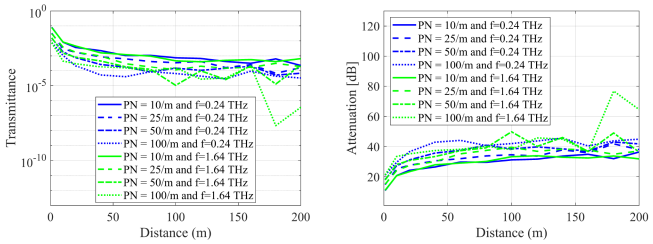

(c) Martian: Transmittance. (d) Martian: Attenuation (dB).

Fig. 6. Simulation measurements of the transmittance and the attenuation for a THz beam of 0.24 THz for Earth ((a) and (b)), and 0.24 THz and 1.64 THz frequency for Mars ((c) and (d)), respectively, by varying the distance between transmitter and the receiver from 1 to 200 m for different particle number (PN) densities of 10/m, 25/m, 50/m and 100/m on the beam propagation path with fixed MCP packets (10000).

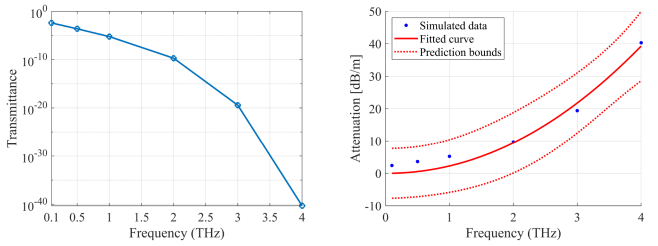

(a) Earth: Transmittance. (b) Earth: Attenuation (dB/m).

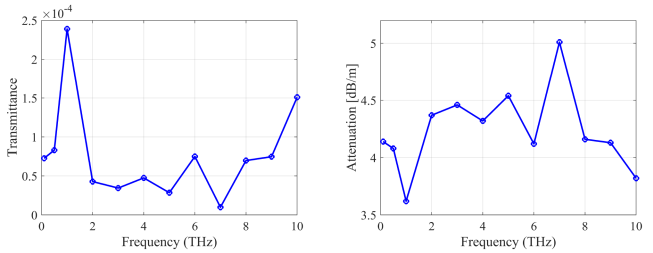

(c) Martian: Transmittance. (d) Martian: Attenuation (dB/m).

Fig. 7. Simulation for a THz beam by varying the frequency from 0.1 to 10 THz while fixing dust particle number (100) on the beam propagation path, MCP packets (10000), and the distance (10 m) between the transmitter and the receiver.

for data transmission. The corresponding attenuation for the transmittance on Earth increases following a power function that can be fitted as $\text{Attenuation}(dB/m) = 2.277 D_{PN}^{2.054}$. On the other hand, the transmittance and attenuation for the Mars environment do not show a particular increase or decrease trend. However, we noticed that the attenuation varies around 4.2 dB/m with the frequency increase from 0.1 to 10 THz.

Finally, we investigated the effect of time-dependent turbulence on the transmittance and the attenuation of the THz signal on Earth and Mars, which corresponds to the 0.24 THz link on Earth and 0.24 and 1.64 THz links on Mars. The distance between the transmitter and the receiver is set to 10 m. Here, we compare Earth and Mars simulation scenarios in which we assume that the dust particle number on the beam propagation path will suddenly increase due to the unpredictable behaviour of wind after 5 s. In the first 5 s, we assume that the dust particle number on the beam will vary between 10-20 in the Earth environment and 100–200 in the Mars environment in clear sky conditions. After five seconds, the dust particle number on the beam will increase between 100–200 on Earth and 10000–20000 on Mars due to the sudden wind turbulence in the communication area. As demonstrated in Fig. 8(a), dust particle number on the beam propagation path is low in the first 5 s compared to the next 5 s for both environments. Also, the dust particle number is higher for the Martian environment than the Earth environment in the considered time interval. Also, the randomly generated dust particle number at 0.24 THz is almost equal to the particle count at 1.64 THz. When observing the transmittance (see Fig. 8(b)), we can notice that it drops suddenly after 5 s for both environments. However, the average transmittance values are approximately similar within the first 5 s. Also, the transmittance on Mars after the turbulence is significantly lower compared to Earth. The attenuation (see Fig. 8(c)) increases dramatically after 5 s and is high on Mars, concluding that the turbulence effect on Mars should be investigated thoroughly. In addition, the transmittance and attenuation differences before and after the turbulence are highly affected by the dust particle number differences. We can conclude that, a slight dust particle number increase dramatically reduces the transmittance for certain frequencies.

B. Channel Capacity Simulation for Earth and Mars Under Dust Storm

This subsection investigates the channel capacity measurement of the THz links considering two scenarios and the influence of high molecular absorption on our model. In the first scenario, we assume that there are time windows when the number of dust particles on the THz beam propagation path drops, creating opportunities to communicate with high data rates for both Earth (0.24 THz) and Mars (0.24 & 1.64 THz) environments. Here we analyse the channel capacity for Earth and Mars environments considering spreading loss and Molecular absorption loss with the THz attenuation due to dust on the beam propagation path. Also, we investigate channel capacity variations in this scenario for different transmitter powers. In the second scenario, we investigate the channel capacity variation with the distance in clear sky and dust storm conditions.

In our first model, we assume that the dust density varies randomly for the Earth environment from 100 and 200 and Mars environment from 10000 to 20000 particles corresponding to a 1 m distance between the transmitter and the receiver. Here we

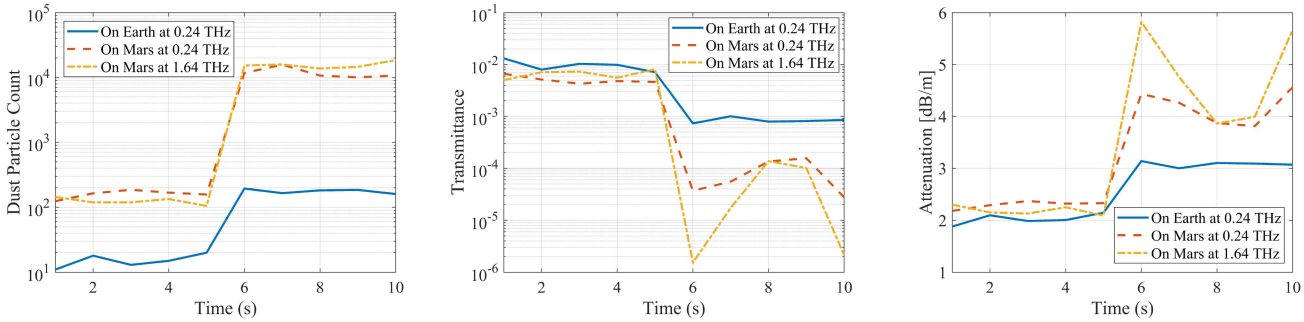

(a) Particle number count. (b) Transmittance. (c) Attenuation (dB/m).

Fig. 8. Comparison of simulations for time-dependent turbulence (after 5 seconds) corresponding to the measurements of a) particle number count, b) the transmittance, and c) the attenuation (dB/m) for Earth and Mars, respectively.

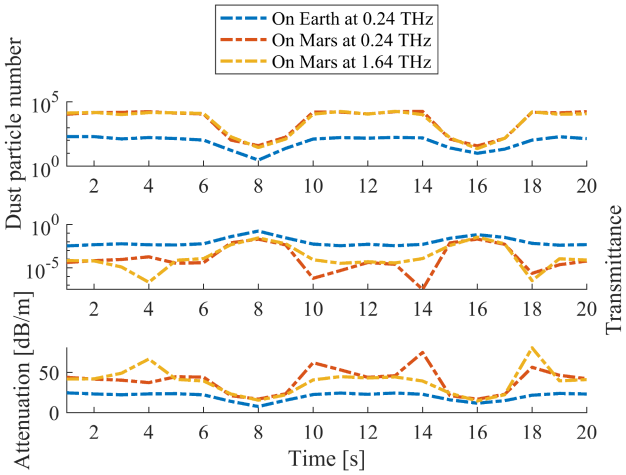

Fig. 9. Measurements of Transmittance and Attenuation of 0.24 THz links for Earth, and 0.24 THz and 1.64 THz for Mars due to the sudden movement of dust particles on the beam propagation path for a fixed transmitter and receiver distance of 1 m.

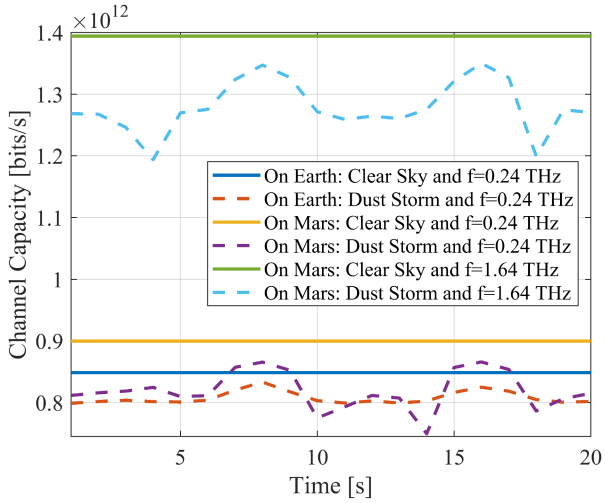

Fig. 10. Channel capacity variation comparison for the scenario of a sudden drop in the number of dust particles on the beam due to the wind behaviour on Earth and Mars environments with considering spreading loss and molecular absorption loss.

acknowledge that considering a 1 m distance for simulation is unrealistic. However, in this scenario, we need to infer the effect of the sudden dust particle drop for the channel capacity. Therefore, it is adequate to consider a 1 m distance for the experiment. As we mentioned above, the significant variation of dust particles on Earth and Mars is in its effective radius. On Earth, the average effective radius of a dust particle varies between 1 and 150 microns [10], and on Mars, it varies between 0.5 to 4 microns [27], [47]. Therefore, to measure transmittance/attenuation considering approximately similar beam-blocking areas by dust particles on both Earth and Mars, we should consider 100 times more dust on Mars than on Earth, following the relationship between dust effective radius and area. Moreover, we sampled the dust particle number for each environment every second for 20 s. In addition, we assume there are two-time intervals (t=[7 s,9 s], t=[15 s,17 s]) when the dust particle number drops to less than 30 and 300 particles (see Fig. 9) due to the unpredictable behaviour of wind on Earth and Mars, respectively. Such time intervals might represent occasions when the wind that causes dust particles to be suspended in the atmosphere falls away to near zero.

Furthermore, as we can see from Fig. 9, the relative dust particle density decrease at the interval centred on t=16 s is much higher than at the interval centred on t=8 s for both environments. Moreover, the transmittance is higher at the interval 15–17 s than at the 7–9 s interval corresponding to the low dust density as expected, and the attenuation shows the opposite variation to transmittance. In principle, those time intervals represent attractive time windows for communication in both environments because of lower attenuation due to the momentary absence of dust particles in the channel.

Fig. 10 illustrates the channel capacity variation in the clear sky and dust storm conditions on Earth and Mars for the same dusty scenario. When observing Fig. 10, we noticed that in clear sky conditions, the channel capacity on Mars is approximately 0.8995 $\times 10^{12}$ $bits/s$, and on Earth, it is nearly 0.85 $\times 10^{12}$ $bits/s$ at 0.24 THz. The reason for this difference is the presence of high molecular absorption gases (see Table I) and water vapour content in the Earth's atmosphere compared to Mars. However, utilising 1.64 THz, we can reach more than 1.5 times

the channel capacity ($1.39 \times 10^{12}\ bits/s$) on Mars than on Earth, due to the high energy weight of MCP packets and low molecular absorption. Therefore, we can expect approximately 50 GB/s more channel capacity in clear sky conditions on Mars than on Earth at 0.24 THz. Also, utilising a higher THz frequency of 1.64 THz, we can reach more than 500 GB/s extra channel capacity on Mars compared to Earth at 0.24 THz in clear sky conditions. Also, it is noticeable that dust appears to have a more significant relative effect on channel capacity on Mars than on Earth in a storm situation due to the high number of dust particles on the beam propagation path. Moreover, the channel capacity in dust storm situations on Earth is lower than in clear sky conditions, but the difference is minimal compared to Mars. The difference on Mars at 1.64 THz frequency is relatively high, and it is approximately two orders of magnitude less than clear sky conditions. On the other hand, the channel capacity in dust storm conditions on Mars is higher by approximately five orders of magnitude than dust storm conditions on Earth at 0.24 THz. We also notice a similarity between the channel capacity on Earth and Mars at 0.24 THz, but at certain time points, the difference goes up to 20 GB/s. In addition, the free space path loss is constant in this scenario because it only depends on the carrier frequency and the distance between the transmitter and the receiver, which are both constant in this simulation process.

In Fig. 11, we investigated the channel capacity measurement variations for different transmitter power in discrete time windows considering the free space path loss and the molecular absorption loss effect on the channel. This figure shows that the channel capacity increases as the antenna transmitter power increases for both environments by approximately 5 to 20 GB/s on Earth at 0.24 THz, 6 to 21 GB/s on Mars at 0.24 THz and 9 to 30 GB/s at 1.64 THz. Moreover, the difference in channel capacity on Earth and Mars at 0.24 THz frequency varies from 5 to 53 GB/s for the corresponding transmitter power. In addition, the channel capacity differences corresponding to each transmitter power vary from 35 to 53 GB/s when comparing the 0.24 and 1.64 THz frequencies on Mars. Also, we noticed that we can have reliable communication links with higher channel capacities when communicating in the time windows with low dust densities on Mars. Moreover, the channel capacity shows a significant variation on Earth compared to Mars for all transmitted powers. Furthermore, comparing the average channel capacity of 8.0771 $\times 10^{11}\ bits/s$ on Earth, utilising an antenna with a 10 dBm transmitter power, to the channel capacity of 8.1 $\times 10^{11}\ bits/s$ on Mars at 0.24 THz, using a 1 dBm antenna, it can be inferred that lower transmitter power antennas can achieve higher channel capacities on Mars compared to Earth.

In our second simulation scenario, we investigated the channel capacity for various distances between the transmitter and the receiver for both Earth and Mars environments, comparing clear sky and dust storm conditions with different dust densities per meter (See Fig. 12). The transmitter power was taken as 10 dBm in this simulation. Here, we allowed the dust particle count density to vary as a factor of distance to simulate more realistic dust storm conditions. For the Earth's environment, we have considered dust storms that result in 10–20 (very low) and

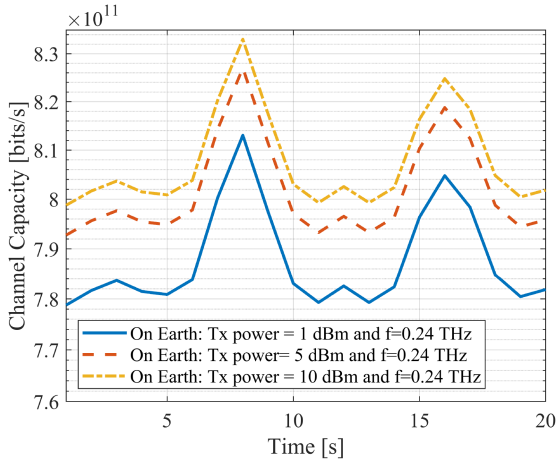

(a) On Earth

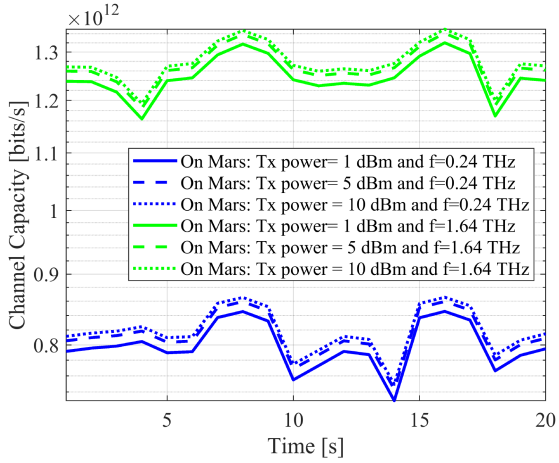

(b) On Mars

Fig. 11. Channel capacity measurement variation for the scenario of a sudden drop in the number of dust particles on the beam due to the wind behaviour for different Transmitter (Tx) powers ($1, 5, 10\ dBm$) of the antenna with considering spreading and molecular absorption (a) on Earth and (b) on Mars.

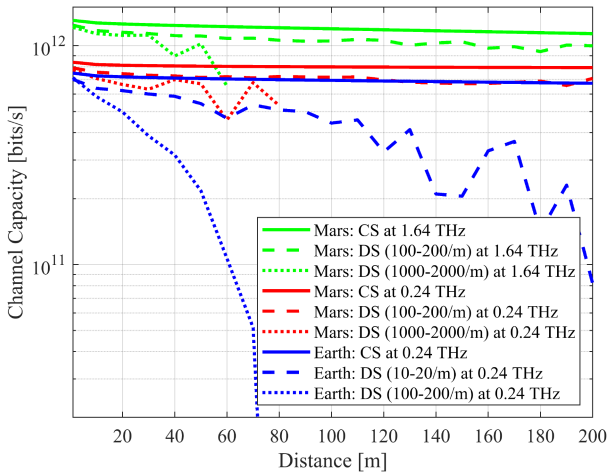

Fig. 12. Channel capacity measurements by varying the distance between the transmitter and the receiver with and without dust storms situations on Mars and Earth at 0.24 THz and 1.64 THz frequencies (CS: Clear Sky, DS: Dust Storm).

100–200 (very high) dust particles per meter dust densities on the THz beam propagation path. Similar conditions for the Mars environment were considered by comparing the dust particle sizes with Earth. Thus, we assumed that dust storms on Mars would carry 100-200 and 1000–2000 dust particles per meter to the beam propagation path. However, we should have considered 10000–20000 dust particles per meter on Mars. Nevertheless, due to computational difficulties with high dust densities with increasing the distance between the transmitter and the receiver, we are considering above mentioned numbers for the channel capacity. Moreover, we have taken account of spreading loss and molecular absorption loss when calculating the channel capacities for each distance.

As shown in Fig. 12, the channel capacity decreases gradually for clear sky conditions for both environments showing high channel capacities in the low molecular absorption frequencies of 0.24 on Earth, and 0.24 and 1.64 Mars in the considered distance range. However, the decrement is high on Earth due to high molecular absorption compared to Mars. When comparing the channel capacity differences in clear sky conditions on Earth and Mars for the considered frequencies, we noticed an $average$ of 100 GB/s difference between Earth and Mars at 0.24 THz, 500 GB/s difference between measurements at 0.24 THz on Earth and 1.64 THz on Mars, and 400 GB/s difference at 0.24 THz and 1.64 THz on Mars. Moreover, the channel capacity decreases dramatically on Earth with the distance for 100-200/m dust storm conditions, showing communication blackout beyond 70 m distance. Also, at 10-20/m dust storms, channel capacity decreases slowly, showing that this dust particle number on the beam propagation path is not a massive issue for achieving high channel capacities for the different distance ranges. However, Earth's channel capacity drops significantly when compared with Mars for the 100-200/m dust particle density for both frequencies 0.24 and 1.64 THz. Again, 100-200/m dust particles on the beam propagation path on Mars do not significantly affect the channel capacity at both frequencies. Therefore, we can neglect the THz link budget degradation due to the small amount of dust ($x < 200/m$) on Mars. We can observe that the channel capacity for Mars decreases rapidly with the increase in the distances when a high number of dust particles are present on the beam propagation path. Furthermore, we notice that channel capacities are on average equal in the clear sky conditions on Earth and 100–200/m dust storm conditions on Mars, implying that we can match the expected channel capacities on Earth even in the dust storm conditions on Mars.

C. Influence of High Molecular Absorption

In this study, our main focus is to investigate the THz EM links communication through a dust storm condition on Earth and Mars. Therefore, we have chosen low molecular absorption frequencies of 0.24 THz for Earth and 0.24 and 1.64 THz for Mars in this study. Our aim is to see the total impact of the THz link caused by the dust particles on the beam propagation path. In this sub-section, we discuss the influence of molecular absorption on our model, and this discussion will explain the reason for selecting these specific frequencies.

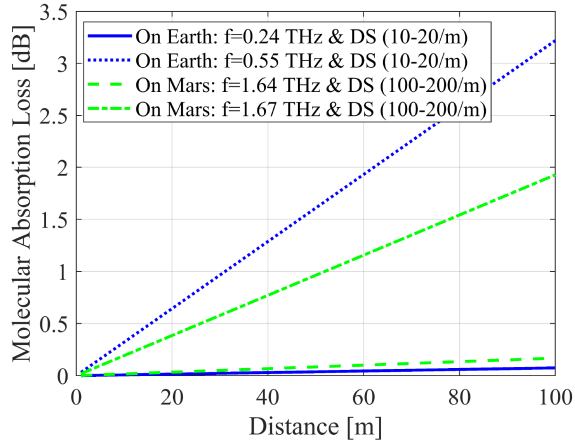

(a) Molecular Absorption Loss

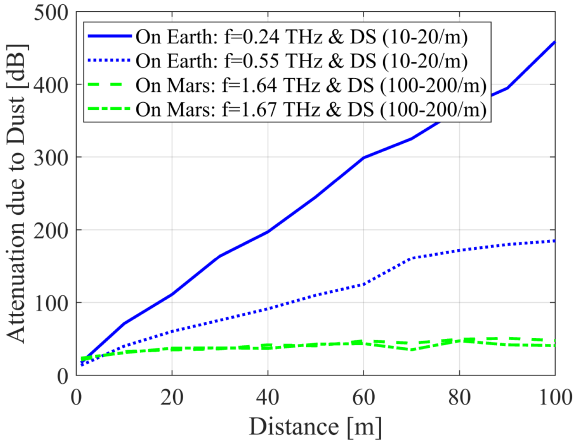

(b) Attenuation due to Dust Storms

Fig. 13. Molecular absorption and attenuation due to dust storms at 0.24 and 0.55 THz on Earth, and at 1.64 and 1.67 THz on Mars (DS: Dust storm).

According to the literature, at 0.24 THz [44], [45], [46] and 0.55 THz [31] frequencies, in Earth's atmosphere, and at 1.64 THz and 1.67 THz [20] on Mars, we expect low and high molecular absorption, respectively. Also, we assumed that dust density on the beam propagation path on Earth is 10-20/m and 100-200/m on Mars. Since we are utilising low and high molecular absorption frequencies for this analysis, Fig. 13(a) clearly demonstrates variations as we expected. On Earth, the high molecular absorption frequency link (i.e. 550 GHz) is highly affected by the water vapour and other gases mentioned in Table I. The Earth's molecular absorption losses are severe with respect to the distance when we compare with Mars at 1.67 THz. The results are opposite when we compare to the 0.24 THz link on Earth and the 1.64 THz link on Mars, due to the higher frequency and dust density on the beam propagation path. When investigating Fig. 13(b), we can see a completely different behaviour for attenuation due to the dust in these environments for the specific frequencies. Attenuation due to dust on the beam propagation path is higher on Earth than on Mars, and low molecular absorption frequencies show higher attenuation than

high molecular absorption frequencies. Moreover, even Earth's attenuation at 0.24 and 0.55 THz show a dramatic increase in the attenuation differences with the distance. However, the attenuation on Mars is approximately equal, with less difference. Hence, in future studies concerning attenuation due to dust in THz links, it is recommended to carefully select a frequency with low molecular absorption.

VII. Conclusion

High-speed, reliable communication between devices on Earth and Mars is needed to fulfil future communication requirements. In this study, we investigated the impact of atmospheric dust and dust storms for communication using THz links, utilising a modified Monte Carlo simulation algorithm. The calculated transmittance and the attenuation based on Mie and Rayleigh approximations depend on the dust particle sizes and carrier frequency utilised for communication on the two planets. Moreover, we presented a channel capacity model and analysed it for two different time-dependent and distance-dependent scenarios. The Monte-Carlo simulation results show that the attenuation decreases for both Earth and Mars environments when the MCP packets and visibility increase. In addition, for both environments, the attenuation increases with higher dust particle number on the beam propagation path and distance between the transmitter and the receiver. We noticed the exact attenuation behaviour with increased frequency for the Earth's environment. However, the attenuation varies around a constant value for the Mars environment. When investigating the channel capacity from the time-dependent scenario, we can conclude that the time windows showing sudden dust particle density drops create the best communication opportunities with high data rates. Also, we noticed that the channel capacity dramatically drops with the increase in distance between the transmitter and the receiver in severe dust storm situations on both Earth (100–200/m) and Mars (1000–2000/m) environments at the relevant frequencies, even if we use low molecular absorption frequencies and high transmitter power antennas. However, the impact from the local dust storm is negligible on Mars (100–200/m) but should be further investigated on Earth (10–20/m).

References

[1] A. Shafie, G. N. Yang, C. Han, J. M. Jornet, M. Juntti, and T. Kurner, "Terahertz communications for 6G and beyond wireless networks: Challenges, key advancements, and opportunities," *IEEE Netw.*, 2022, early access, pp. 1–8, Sep. 12, 2022, doi: 10.1109/MNET.118.2200057.

[2] I. F. Akyildiz, C. Han, Z. Hu, S. Nie, and J. M. Jornet, "Terahertz band communication: An old problem revisited and research directions for the next decade," *IEEE Trans. Commun.*, vol. 70, no. 6, pp. 4250–4285, Jun. 2022.

[3] C. Han et al., "Terahertz wireless channels: A holistic survey on measurement, modeling, and analysis," *IEEE Commun. Surv. Tut.*, vol. 24, no. 3, pp. 1670–1707, Thirdquarter 2022.

[4] D. Serghiou, M. Khalily, T. W. Brown, and R. Tafazolli, "Terahertz channel propagation phenomena, measurement techniques and modeling for 6G wireless communication applications: A survey, open challenges and future research directions," *IEEE Commun. Surveys Tut.*, vol. 24, no. 4, pp. 1957–1996, Fourthquarter 2022.

[5] H. Yuan, N. Yang, X. Ding, C. Han, K. Yang, and J. An, "Cluster-based multi-carrier hybrid beamforming for massive device terahertz communications," *IEEE Trans. Commun.*, vol. 70, no. 5, pp. 3407–3420, May 2022.

[6] A. Shafie, N. Yang, S. A. Alvi, C. Han, S. Durrani, and J. M. Jornet, "Spectrum allocation with adaptive sub-band bandwidth for terahertz communication systems," *IEEE Trans. Commun.*, vol. 70, no. 2, pp. 1407–1422, Feb. 2022.

[7] J. M. Jornet and I. F. Akyildiz, "Graphene-based plasmonic nano-antenna for terahertz band communication in nanonetworks," *IEEE J. Sel. Areas Commun.*, vol. 31, no. 12, pp. 685–694, Dec. 2013.

[8] M. Pengnoo, M. T. Barros, L. Wuttisittikulkij, B. Butler, A. Davy, and S. Balasubramaniam, "Digital twin for metasurface reflector management in 6G terahertz communications," *IEEE Access*, vol. 8, pp. 114580–114596, 2020.

[9] H. Siljak, M. T. Barros, N. D'Arcy, D. P. Martins, N. Marchetti, and S. Balasubramaniam, "Applying intelligent reflector surfaces for detecting violent expiratory aerosol cloud using terahertz signals," *IEEE Netw.*, early access, pp. 1–8, Jul. 25, 2022, doi: 10.1109/MNET.122.2200116.

[10] L. Xie, H. Zhong, Z. Du, and J. Zhou, "Monte Carlo simulation of electromagnetic wave transmittance in charged sand/dust storms," *J. Quantitative Spectrosc. Radiative Transfer*, vol. 241, 2020, Art. no. 106744.

[11] Z. Diao, Q. Jing, and W. Zhong, "Comparison of the influence of martian and Earth's atmospheric environments on terahertz band electromagnetic waves," *Int. J. Commun. Syst.*, vol. 34, no. 12, 2021, Art. no. e4894.

[12] W. Hongxia, S. Honghui, Z. Xuanke, S. Xiaofang, W. Lianfen, and Z. Yunfang, "Simulation of multiple scattering of THz wave propagation in sandstorm," in *Proc. J. Phys.: Conf. Ser.*, 2020, vol. 1437, Art. no. 012033.

[13] K. Su, L. Moeller, R. B. Barat, and J. F. Federici, "Experimental comparison of terahertz and infrared data signal attenuation in dust clouds," *J. Opt. Soc. Amer. A*, vol. 29, no. 11, pp. 2360–2366, 2012.

[14] Z. E. O. Elshaikh, M. R. Islam, O. O. Khalifa, and H. Abd-El-Raouf, "Mathematical model for the prediction of microwave signal attenuation due to duststorm," *Prog. Electromagn. Res. M*, vol. 6, pp. 139–153, 2009.

[15] X. Li, L. Xingcai, and Z. Xiaojing, "Attenuation of an electromagnetic wave by charged dust particles in a sandstorm," *Appl. Opt.*, vol. 49, no. 35, pp. 6756–6761, 2010.

[16] X. Li, X. Min, and D. Liu, "Rayleigh approximation for the scattering of small partially charged sand particles," *J. Opt. Soc. Amer. A*, vol. 31, no. 7, pp. 1495–1501, 2014.

[17] P. Sen et al., "Terahertz communications can work in rain and snow: Impact of adverse weather conditions on channels at 140 GHz," in *Proc. 6th ACM Workshop Millimeter-Wave Terahertz Netw. Sens. Syst.*, 2022, pp. 13–18.

[18] J. Ma, J. Adelberg, R. Shrestha, L. Moeller, and D. M. Mittleman, "The effect of snow on a terahertz wireless data link," *J. Infrared, Millimeter, Terahertz Waves*, vol. 39, no. 6, pp. 505–508, 2018.

[19] I. F. Akyildiz, J. M. Jornet, and C. Han, "TeraNets: Ultra-broadband communication networks in the terahertz band," *IEEE Wireless Commun.*, vol. 21, no. 4, pp. 130–135, Aug. 2014.

[20] L. T. Wedage, S. Balasubramaniam, B. Butler, M. C. Vuran, and Y. Koucheryavy, "Path loss analysis of terahertz communication in Mars' atmospheric conditions," in *Proc. IEEE Int. Conf. Commun. Workshops*, 2022, pp. 1225–1230.

[21] K. Harb, B. Omair, S. Abdul-Jauwad, A. Al-Yami, and A. Al-Yami, "A proposed method for dust and sand storms effect on satellite communication networks," in *Proc. Conf. Innov. Commun. Theory*, 2012, pp. 33–37.

[22] K. Gui et al., "Record-breaking dust loading during two mega dust storm events over northern China in March 2021: Aerosol optical and radiative properties and meteorological drivers," *Atmospheric Chem. Phys.*, vol. 22, no. 12, pp. 7905–7932, 2022.

[23] S. De and A. A. B. Raj, "Experimental study of sand-storm effect on digital FSO communication link," in *Proc. IEEE Int. Conf. Recent Trends Electron., Inf., Commun. Technol.*, 2020, pp. 35–40.

[24] J. Zhou, X. Dou, and L. Xie, "Scattering and attenuation of electromagnetic waves by partly charged particles," *J. Quantitative Spectrosc. Radiative Transfer*, vol. 206, pp. 55–62, 2018.

[25] M. I. Mishchenko, "Gustav mie and the fundamental concept of electromagnetic scattering by particles: A perspective," *J. Quantitative Spectrosc. Radiative Transfer*, vol. 110, no. 14–16, pp. 1210–1222, 2009.

[26] C. Ho, N. Golshan, and A. Kliore, "Radio wave propagation handbook for communication on and around Mars," Nat. Aeronaut. Space Admin., Washington, D.C., USA, Tech. Rep. JPL-Publ-02-5, 2002.

[27] M. Luginin et al., "Properties of water ice and dust particles in the atmosphere of Mars during the 2018 global dust storm as inferred from the atmospheric chemistry suite," *J. Geophys. Res.: Planets*, vol. 125, no. 11, 2020, Art. no. e2020JE006419.

[28] M. Franceschetti, "Stochastic rays pulse propagation," *IEEE Trans. Antennas Propag.*, vol. 52, no. 10, pp. 2742–2752, Oct. 2004.

[29] M. Franceschetti, J. Bruck, and L. J. Schulman, "A random walk model of wave propagation," *IEEE Trans. Antennas Propag.*, vol. 52, no. 5, pp. 1304–1317, May 2004.
[30] J. Paasschens, "Solution of the time-dependent Boltzmann equation," *Phys. Rev. E*, vol. 56, no. 1, 1997, Art. no. 1135.
[31] T. S. Rappaport et al., "Wireless communications and applications above 100 GHz: Opportunities and challenges for 6G and beyond," *IEEE Access*, vol. 7, pp. 78729–78757, 2019.
[32] C. Ho, M. Sue, and N. Golsham, "Martian atmospheric effects on radio wave propagation," NASA Jet Propulsion Laboratory, California Inst, Technol., Pasadena, CA, USA, 2001. [Online]. Available: https://hdl.handle.net/2014/12321
[33] E. K. Smith and W. L. Flock, "Propagation through martian dust at 8.5 and 32 GHz," *Telecommun. Data Acquisition Rep.*, pp. 42–87, 1986.
[34] M. R. Islam, Z. E. O. Elshaikh, O. O. Khalifa, A. Z. Alam, S. Khan, and A. Naji, "Prediction of signal attenuation due to duststorms using MIE scattering," *IIUM Eng. J.*, vol. 11, no. 1, pp. 71–87, 2010.
[35] X. Wenzhong, Z. Kai, M. Jialin, X. Degang, W. Yuye, and Y. Jianquan, "THz wave attenuation characteristics in sand and dust," *Infrared Laser Eng.*, vol. 44, no. 2, pp. 523–527, 2015.
[36] S. M. Sharif, "Attenuation properties of dusty media using MIE scattering solution," *Prog. Electromagn. Res. M*, vol. 43, pp. 9–18, 2015.
[37] D. J. Lockwood, "Rayleigh and MIE scattering," in *Encyclopedia of Color Science and Technology*. Berlin, Germany: Springer, 2016, pp. 1097–1107.
[38] Y.-H. Zhou, Q. Shu He, and X. Jing Zheng, "Attenuation of electromagnetic wave propagation in sandstorms incorporating charged sand particles," *Eur. Phys. J. E*, vol. 17, pp. 181–187, 2005.
[39] X. Liu and J. Schmidt, "Configuration of the martian dust rings: Shapes, densities, and size distributions from direct integrations of particle trajectories," *Monthly Notices Roy. Astronomical Soc.*, vol. 500, no. 3, pp. 2979–2985, 2021.
[40] V. J. Novick, "Use of series light extinction cells to determine aerosol number concentration," *Aerosol Sci. Technol.*, vol. 9, no. 3, pp. 251–262, 1988.
[41] C. Han, A. O. Bicen, and I. F. Akyildiz, "Multi-ray channel modeling and wideband characterization for wireless communications in the terahertz band," *IEEE Trans. Wireless Commun.*, vol. 14, no. 5, pp. 2402–2412, May 2015.
[42] J. M. Jornet and I. F. Akyildiz, "Channel modeling and capacity analysis for electromagnetic wireless nanonetworks in the terahertz band," *IEEE Trans. Wireless Commun.*, vol. 10, no. 10, pp. 3211–3221, Oct. 2011.
[43] I. Gordon et al., "The HITRAN2016 molecular spectroscopic database," *J. Quantitative Spectrosc. Radiative Transfer*, vol. 203, pp. 3–69, Dec. 2017.
[44] P. Sen, J. V. Siles, N. Thawdar, and J. M. Jornet, "Multi-kilometre and multi-gigabit-per-second sub-terahertz communications for wireless backhaul applications," *Nature Electron.*, vol. 6, pp. 164–175, 2022.
[45] S. Koenig et al., "Wireless sub-THz communication system with high data rate," *Nature Photon.*, vol. 7, no. 12, pp. 977–981, 2013.
[46] Z. Chen et al., "A survey on terahertz communications," *China Commun.*, vol. 16, no. 2, pp. 1–35, 2019.
[47] M. Lemmon et al., "Martian dust particle size during the 201.8 planet-encircling dust storm as measured by the curiosity rover," in *Proc. 9th Int. Conf. Mars*, vol. 2089, 2019, Art. no. 6298.

Lasantha Thakshila Wedage (Student Member, IEEE) received the B.S. degree in mathematics from the University of Ruhuna, Matara, Sri Lanka, in 2016. He is currently working toward the Ph.D. degree with the Department of Computing and Mathematics, Walton Institute, South East technological University, Waterford, Ireland. His research interests include mathematical modelling and 5G/6G wireless communication and sensing. (thakshila.wedage@waltoninstitute.ie).

Bernard Butler (Senior Member, IEEE) received the Ph.D. degree from South East Technological University, Waterford, Ireland. He was a Senior Research Scientist with the U.K. National Physical Laboratory, focusing on mathematics of measurement and sensing. He is a Lecturer with South East Technological University(SETU), Waterford, Ireland, and is CONNECT Funded Investigator and VistaMilk Academic Collaborator with the Walton Institute, SETU. Research interests include machine learning, wireless comms and edge networking. (bernard.butler@setu.ie).

Sasitharan Balasubramaniam (Senior Member, IEEE) received the Bachelors degree in engineering and the Ph.D. degree from the University of Queensland, Brisbane, QLD, Australia, in 1998 and 2005, respectively, and the Masters of engineering science from the Queensland University of Technology, Brisbane, in 1999. He was a past recipient of the Science Foundation Ireland Starter Investigator Research Grant. He was also a past recipient of the Academy of Finland Research Fellow with Tampere University, Finland. He was previously the Director of Research at the Walton Institute, South East Technological University, Ireland. He is currently an Associate Professor with the School of Computing, University of Nebraska-Lincoln, Lincoln, NE, USA. His research interests include molecular and nano communications, Internet of Bio-Nano Things, and 5G/6G networks. He is currently the Editor-in-Chief of IEEE TRANSACTIONS ON MOLECULAR, BIOLOGICAL AND MULTI-SCALE COMMUNICATIONS and an Associate Editor for IEEE TRANSACTIONS ON MOBILE COMPUTING. He was an IEEE Distinguished Lecturer for the IEEE Nanotechnology Council in 2018. (sasi@unl.edu) .

Yevgeni Koucheryavy (Senior Member, IEEE) received the Ph.D. degree from the Tampere University of Technology, Tampere, Finland, in 2004. He is currently a Full Professor with the Unit of Electrical Engineering, Tampere University. He has authored numerous publications in the field of advanced wired and wireless networking and communications. His research interests include various aspects in heterogeneous wireless communication networks and systems, the Internet of Things and its standardization, and nanocommunications. (yevgeni.koucheryavy@yl-verkot.com).

Mehmet C. Vuran (Member, IEEE) received the B.Sc. degree in electrical and electronics engineering from Bilkent University, Ankara, Turkey, in 2002, the M.S. and Ph.D. degrees in electrical and computer Engineering from the Georgia Institute of Technology, Atlanta, GA, USA, in 2004 and 2007, respectively. He is currently the Dale M. Jensen Chair Professor of Computing with the School of Computing, University of Nebraska-Lincoln, Lincoln, NE, USA. Dr. Vuran has been recognized as a Highly Cited Researcher three years in a row by Thomson Reuters in recognition of ranking among the top 1% of researchers for most cited documents in Computer Science. Dr. Vuran was the recipient of the NSF CAREER award for the project "Bringing Wireless Sensor Networks Underground". He is a Daugherty Water of Food Institute Fellow and a National Strategic Research Institute Fellow. He is on the Editorial boards of IEEE TRANSACTIONS ON WIRELESS COMMUNICATIONS, IEEE TRANSACTIONS ON MOBILE COMPUTING, and IEEE TRANSACTIONS ON NETWORK SCIENCE AND ENGINEERING. His research interests include 6G networks, the Internet of Things (IoT), agricultural wireless networks, wireless underground communications, and vehicular communications. (mcv@unl.edu).